Supporting Information for

Ultrafast structural evolution and formation of linear carbon chains in single-walled carbon nanotube networks by femtosecond laser irradiation

Jeonghong Ha,[†] Hyun Young Jung,[‡] Ji Hao,[§] Bo Li,[∥] Aldo Raeliarijaona,[⊥] Jorge Alarcón,[⊥] Humberto Terrones,[⊥] Pulickel M. Ajayan,[∥] Yung Joon Jung,*[,§] Jaegu Kim[#] and Dongsik Kim*[,†]

[†]Department of Mechanical Engineering, POSTECH, Pohang, 790-784, Republic of Korea

[‡]Department of Energy Engineering, Gyeongnam National University of Science and Technology, Jinju, 660-758, Republic of Korea

[§]George J. Kostas Research Institute for Homeland Security and Department of Mechanical and Industrial Engineering, Northeastern University, Boston, Massachusetts 02115, USA

[∥] Department of Mechanical Engineering and Materials Science, Rice University, Houston, TX 77005, USA

[⊥]Department of Physics, Applied Physics and Astronomy, Rensselaer Polytechnic Institute, 110 Eight Street, Troy, NY 12180, USA

[#]Korea Institute of Machinery and Materials, Daejeon, 305-343, Republic of Korea

Table of Contents

1. Experimental details

1.1 Sample preparation

The SWCNT (signle-walled carbon nanotube)-DI(deionized) water solutions (CNTRENE^{TM} C100, 0.23 wt %) was purchased from Brewer Science.[1] The SWCNTs were surfactant-free but functionalized with carboxylic acid groups for stable dispersion. The defects on the surface may help the formation of MWCNTs, but their role in the coalescence process along with the physical mechanism is not fully understood yet.

The SWCNT network sample was fabricated on SiO_2/Si substrates by the template-guided fluidic assembly method.[2] First, the SiO_2/Si substrate was treated by inductively coupled plasma (ICP) for 5 s to improve the hydrophilic property of its surface. Second, the substrate was patterned to build the trench structures by using the standard optical lithography technique. Third, the sample was vertically dipped into the SWCNT / DI-water solution along the direction of trenches using a dip coater, and then pulled off the solution at a constant speed of 0.1 mm/min. Fourth, the photoresist on the sample was removed by acetone and further cleaned by Isopropyl Alcohol (IPA)/DI water. Finally, the sample was dried in nitrogen atmosphere.

The SWCNTs in the fabricated SWCNT network are bonded by the Van der Waals force. Based on our evaluation, the density of SWCNTs is up to 2×10^{12} cm^{-2}. As the SWCNT solution we purchased is mixed type, both metallic and semiconducting SWCNTs are included with a ratio of 2:1. Therefore, the junction types between SWCNTs can be metallic/metallic, metallic/semiconducting, and semiconducting/semiconducting. Most of the SWCNTs in our sample have random orientation, but those close to the strip edges are aligned along the assembly direction.[3] In this work, the effect of orientation of the CNTs can be neglected, since all the experiments were done in the middle of the CNT strip. We expect that better alignment and higher density of CNTs can increase the possibility of coalescence significantly.

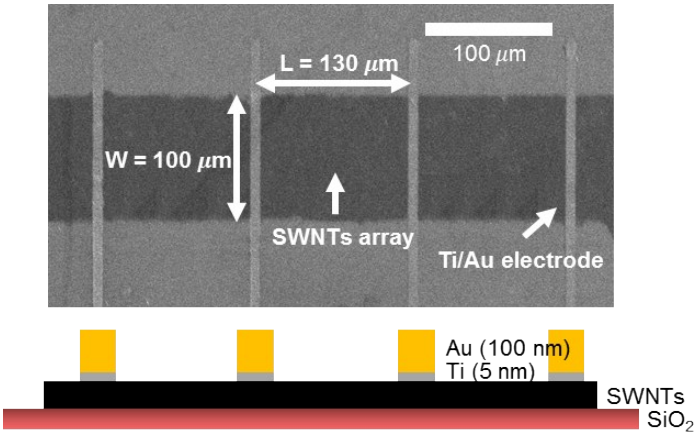

Figure S1 | SWNT device. A SEM image (top) shows a SWNT device for electrical resistance measurement and the schematic cross-section of the device.

1.2 Laser treatment

After the sample preparation, the assembled SWNT arrays were irradiated with a Ti:sapphire femtosecond laser (wavelength = 800 nm, full width half maximum = 50 fs, pulse energy < 3 mJ, repetition rate = 1 kHz) under high vacuum (10^{-4} Torr). The incident laser pulse energy was adjusted using a half-wave plate and a polarizer (Fig. S2). The CNTs were randomly deposited and it was assumed that the polarization effect was negligible. After passing through a circular aperture of diameter 1 mm, the laser beam was focused by a lens of focal length 50 mm. The laser spot size (90 μm) was set slightly smaller than the distance between the two adjacent electrodes (130 μm) to prevent the potential damage to the electrodes by the laser irradiation. The CNT arrays were placed horizontally and the laser beam was incident perpendicular to the sample (normal incidence to the surface). The laser pulse number (N_p) was varied up to 100000 at a fixed laser fluence F to induce structural evolution.

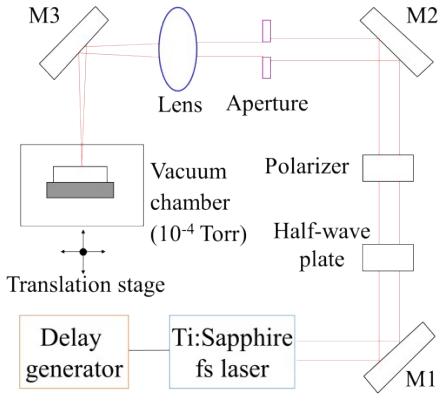

Figure S2 | Experimental setup. Schematic diagram of experimental setup.

1.3 TEM and Raman analysis

The structural change of the transformed nanocarbons were investigated by Raman spectroscopy (LabRAM HR 800, HORIBA Jobin Yvon, HORIBA) using an excitation wavelength of 532 nm. The exposure time was 5 s per spectrum, and the number of data accumulation was 10. The measurements were repeated 10 times in the whole region of the fs laser spot. High-resolution transmission microscope (TEM, JEOL JEM-2200FS) was employed at an accelerating voltage of 200 kV. To avoid the effects of the substrate on Raman results, we transferred the laser-treated SWNTs from silicon substrates to TEM grids using the wet-contact prnigting method.

1.4 Electrical conductivity measurement

The electrical conductivity and thickness of CNT networks were measured by using a 4-wire resistance measurement system and an atomic force microscope (Dimension 3100, VEECO Digital Instruments), respectively. The resistance of the SWNTs network was measured using a multimeter (34401A Multimeter, Agilent). The four-wire probing technique was employed to avoid the effect of the contact resistance between CNT arrays and metal pads.[4] Electrical conductivity (σ) was obtained from the measured resistance (R_{CNT}) (Figs. S3 and S4):

$$\sigma = 1/\rho = l/(AR_{CNT}), \quad (1)$$

where ρ is resistivity, l the length, and A the cross-sectional area of an array (average thickness multiplied by the width of a CNT array).

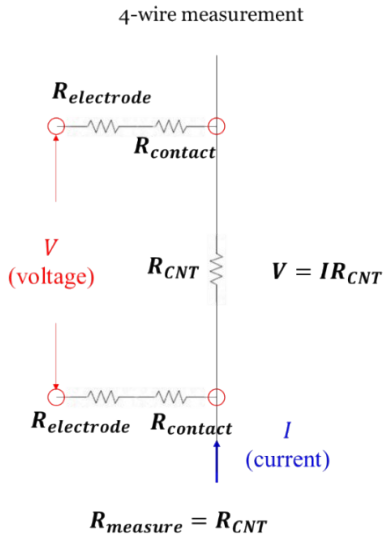

Figure S3 | 4-wire resistance. Electrical circuit to measure the electrical conductivity of CNT

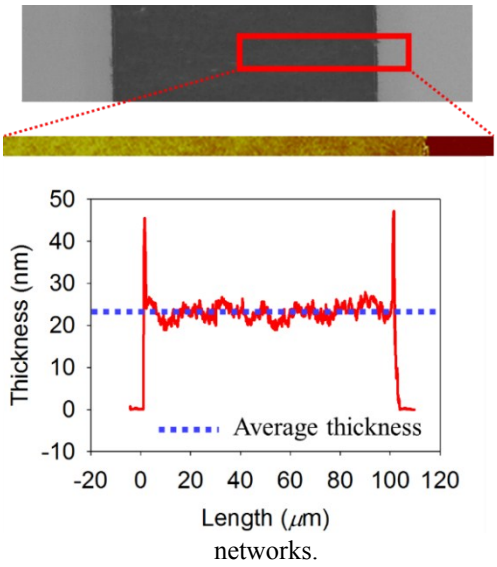

networks.

Figure S4 | AFM analysis. A SEM image with an AFM profile (top) of the SWNT array. The thickness profile along the width direction of the CNT array is shown in the bottom.

In the case of thin films, the electrical conductivity σ_{dc} increase with the thickness t according to percolation theory[5]:

$$\sigma_{dc} = \sigma_o (t\text{-}t_c)^{\alpha}, \quad (2)$$

where σ_{dc} is a constant, t_c the percolation threshold, and α an exponent. In Figure S5, the lines represent the linear fitting of Eq. (2) to the exerimental data (σ_o=1.4 × 10^4 S/m, α = 0.68, and t_c = 1.23 nm at N_p = 100000), which show good agreement with the percolation theory. The electrical

conductivity of 6 devices with different CNT layer thicknesses are displayed in Figure S5.

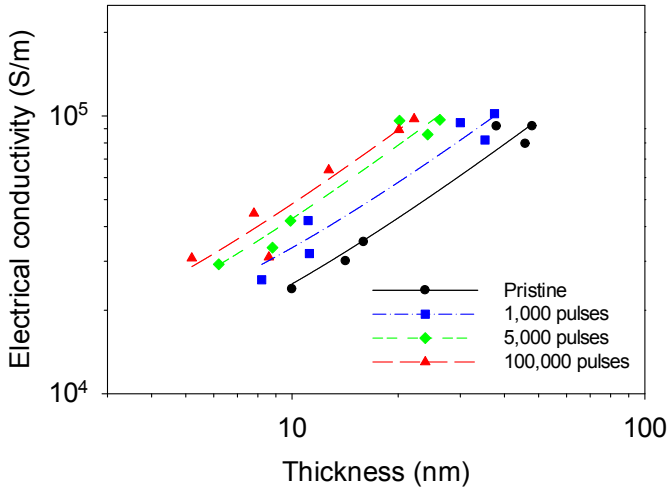

Figure S5 | Electrical conductivity. Electrical conductivity of the CNT layers measured by the 4-wire method. The lines represent linear data fitting using Eq. (2).

1.5 Computational details

Density functional theory calculations were carried out with the plane wave code Quantum Espresso under LDA using density functional perturbation theory (DFPT). The chains where relaxed in boxes leaving at least 15 Å of vacuum to avoid interactions between the chains with a force tolerance of 2.6 × 10^{-5} eV/A and energy difference of 1.4 × 10^{-9} eV. The results where compared to experimental Raman data for acetylene, benzene and methane and showed good agreement.

2 Supplementary Results

2.1 Raman spectra

Figure S6 shows the Raman spectra of the CNT samples before and after laser treatment at various pulse numbers (N_p) and laser fluences (F). The intensity ratio of D band to G band was used to analyze crystallinity of sp^2 nanocarbon materials. At all laser fluences, the coalescence-induced mode (CIM) began to appear when N_p > 1000 and the intensity ratio of CIM to G band (I_{CIM}/I_G) increased with N. The highest I_{CIM}/I_G ~1.6 was obtained at N = 100000 and F = 65 mJ/cm^2.

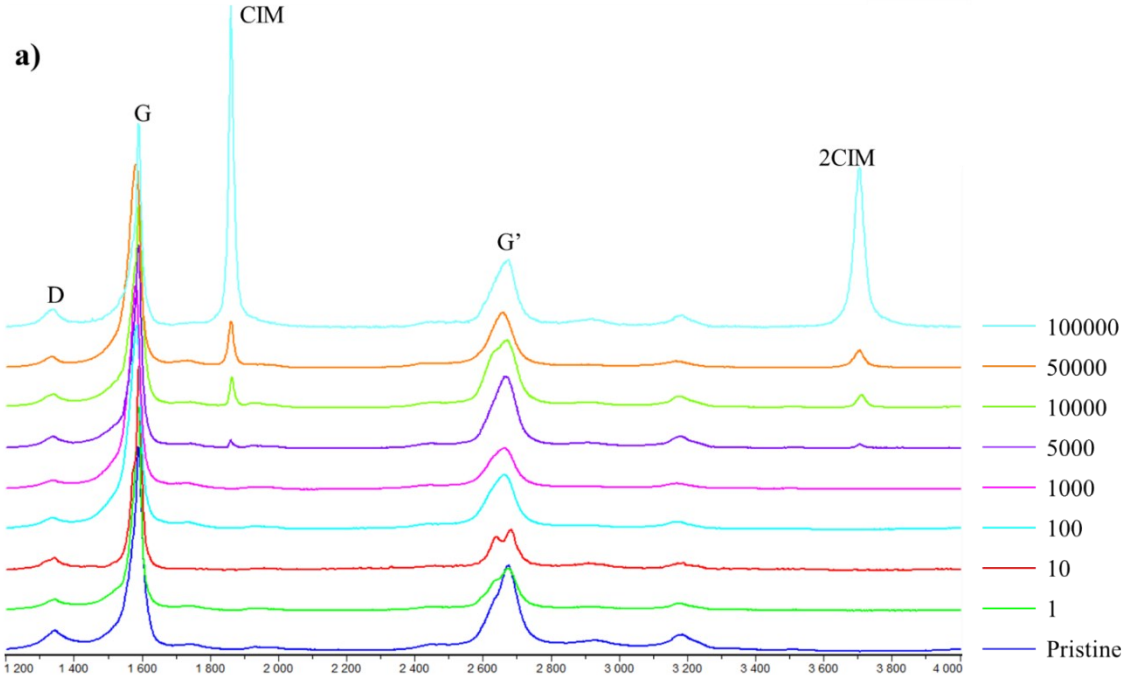
a)
CIM
G
2CIM
G'
D
100000
50000
10000
5000
1000
100
10
1
Pristine
1 200
1 400
1 600
1 800
2 000
2 200
2 400
2 600
2 800
3 000
3 200
3 400
3 600
3 800
4 000

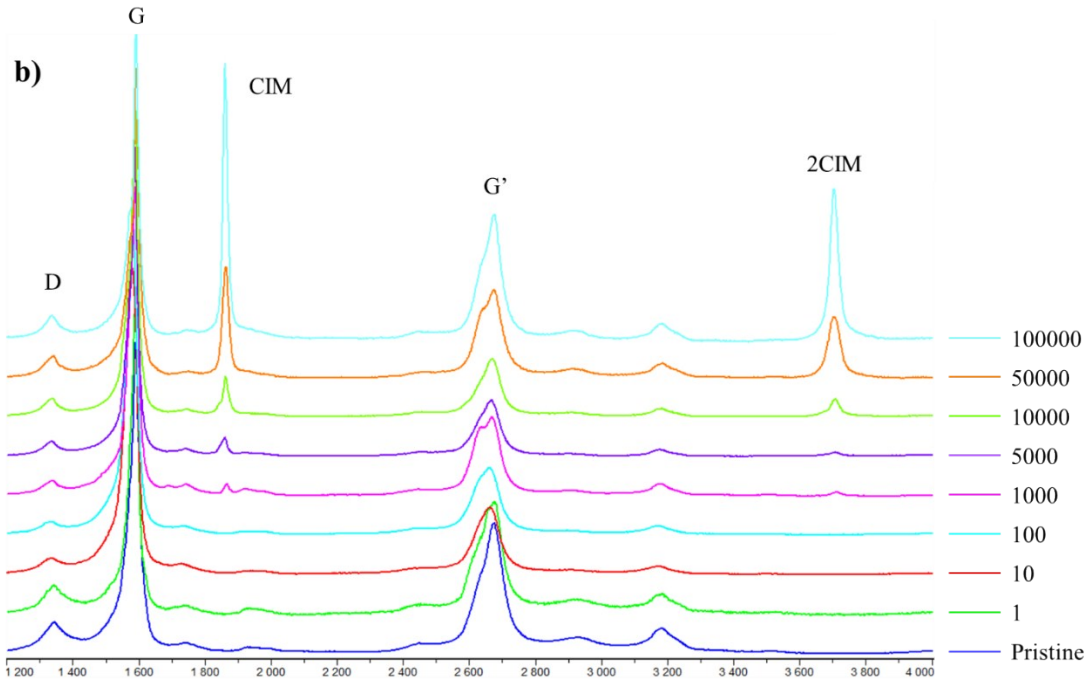
b)
G
CIM
2CIM
G'
D
100000
50000
10000
5000
1000
100
10
1
Pristine
1 200
1 400
1 600
1 800
2 000
2 200
2 400
2 600
2 800
3 000
3 200
3 400
3 600
3 800
4 000

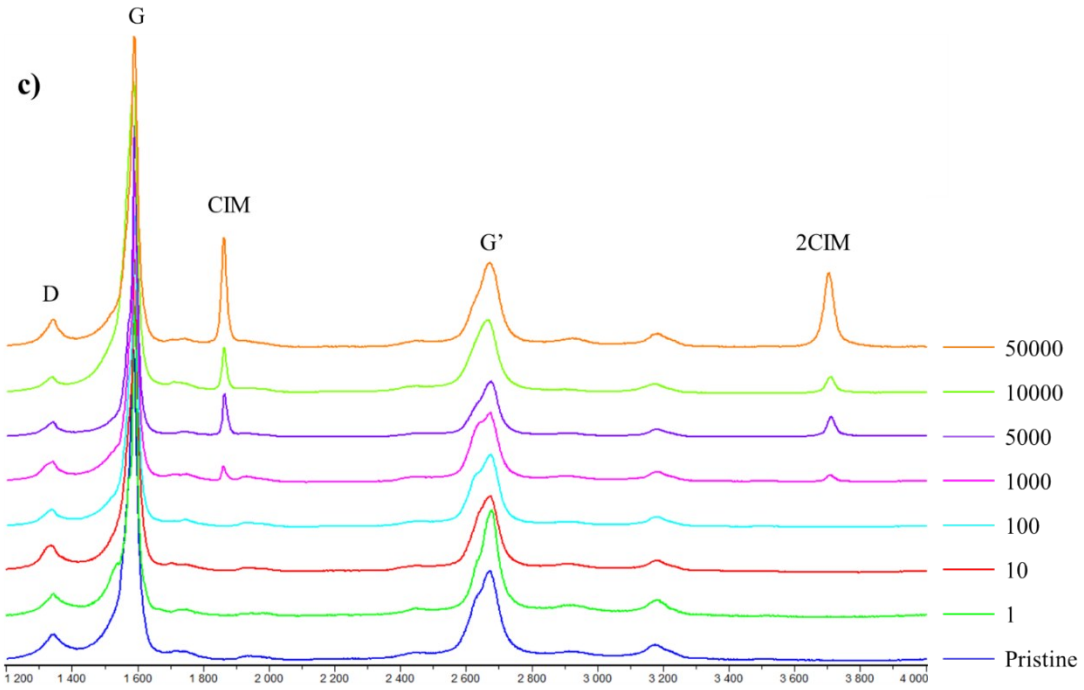
c)
G
CIM
G'
2CIM
D
50000
10000
5000
1000
100
10
1
Pristine
1 200
1 400
1 600
1 800
2 000
2 200
2 400
2 600
2 800
3 000
3 200
3 400
3 600
3 800
4 000

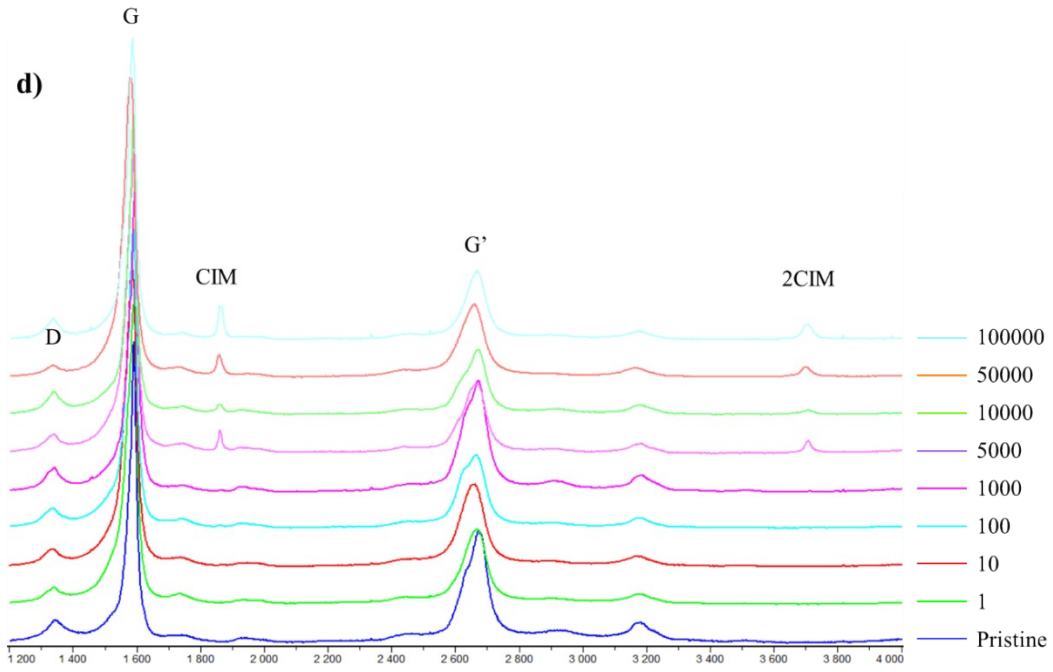
d)
G
G'
CIM
2CIM
D
100000
50000
10000
5000
1000
100
10
1
Pristine
1 200
1 400
1 600
1 800
2 000
2 200
2 400
2 600
2 800
3 000
3 200
3 400
3 600
3 800
4 000

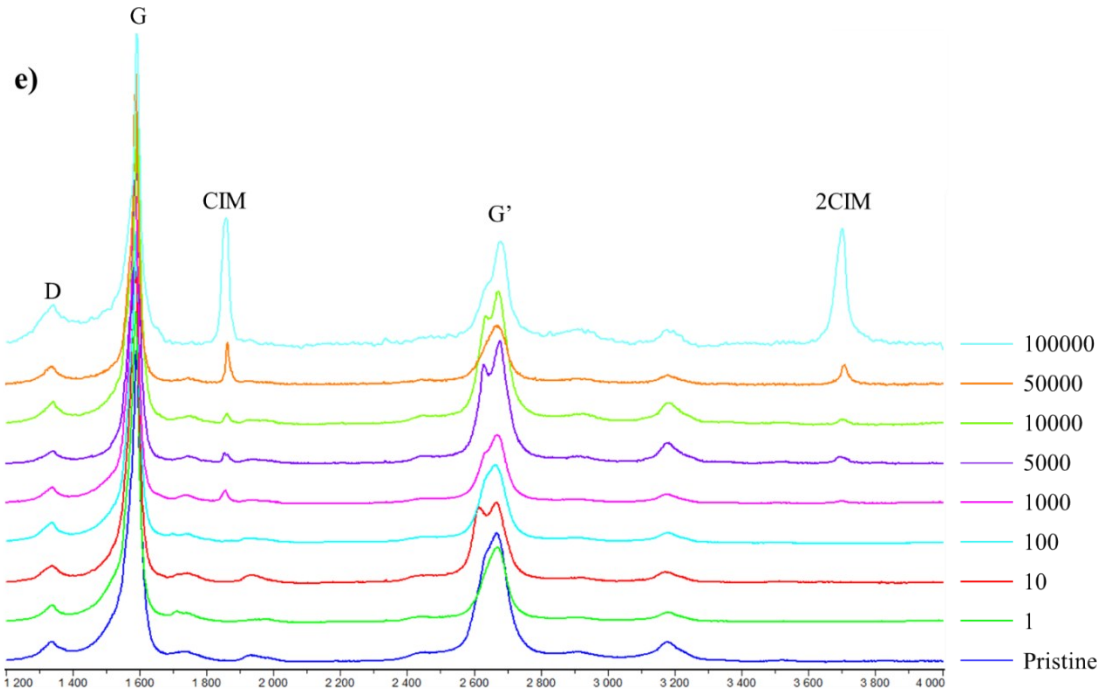

Figure S6 | Raman spectra. Raman spectra before and after the laser irradiation at various pulse numbers and laser fluences: (a) F = 65 mJ/cm^2, (b) F = 98 mJ/cm^2, (c) F = 147 mJ/cm^2, (d) F = 196 mJ/cm^2, and (e) F = 229 mJ/cm^2.

2.2 Dependence of Raman excitation wavelength

Figure S7a shows the Raman spectra obtained at E_{laser} = 2.41 eV (514 nm), 2.33 eV (532 nm), 1.96 eV (633 nm) and 1.58 eV (785 nm). The intensity of CIM was ~1.8 at E_{laser} = 2.41 eV while it was only ~0.02 at E_{laser} = 1.96 eV. The CIM peak was not observed at E_{laser} = 1.58 eV (Figs. S7b and S7c).

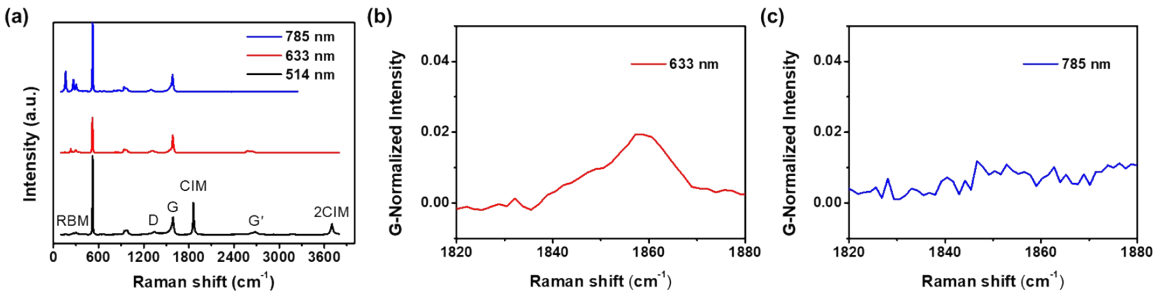

Figure S7 | Raman spectra. Raman spectra obtained at different Raman excitation wavelengths (514, 633, 785 nm) after laser irradiation at F = 98 mJ/cm^2 and N_p =100,000.

2.3 Morphological change of the CNT array

Figure S8 displays the typical SEM images of the CNT array before and after the laser transformation process. At higher fluences (F = 147 mJ/cm^2 and 229 mJ/cm^2), the CNTs have been ablated without maintaining a network. Therefore, we focused on the conditions below F < 100 mJ/cm^2.

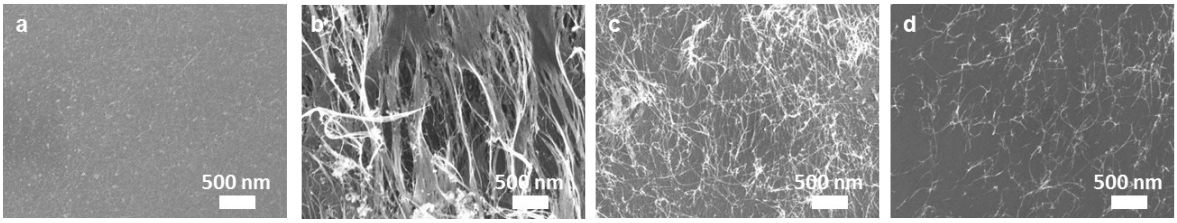

Figure S8 | SEM images of the CNT arrays. SEM images of the CNT arrays (a) before and after laser treatment at (b) F = 98 mJ/cm^2 (c), F = 147 mJ/cm^2, and (d) F = 229 mJ/cm^2 at a fixed N_p = 1000.

2.4 Numerical simulation of temperature evolution by fs laser irradiation

The two-temperature model was employed to estimate the temporal evolution of electron temperature T_e and lattice temperature T_l of the CNT arrays: [6]

$$C_e(T_e)\frac{dT_e}{dt} = \nabla(k\nabla T_e) - G(T_e, T_l) + S(x,t)$$

$$C_l(T_l)\frac{dT_l}{dt} = G(T_e, T_l)$$

where C_e (J/m^3 · K) is the electronic heat capacity, t is time, k_e (W/m · K) is the electronic thermal conductivity, $G(T_e, T_l)$ (W/m^3 · K) is the electron-phonon coupling coefficient, $S(\mathbf{r},t)$ is the heat source for the absorbed laser energy, $\mathbf{r}$ is the position vector, and C_l is the lattice heat capacity. For SWNTs, C_l = (1.37 × 10^6 J/m^3 · K), C_e=C_l/100, and G = 2.0 × 10^{16} W/m^3 · K was used.[6,7] We note that T_e reached in our simulation T_e ≈ 20,000 K, while T_l which initially was 300 K increased due to electron-phonon coupling to reach T_l ≈ 800 K (Fig. S9). This result is consistent with the theoretical work which has confirmed that femtosecond laser irradiation can fragment carbon nanotubes and lead to a large tear in the CNT wall and to formation of linear carbon chains.[8,9] The thermal equilibrium between T_e and T_l was reached in ~3 ps. After the equilibrium, the lattice temperature further decreased by heat diffusion and the thermal relaxation time, which is the time taken for the temperature to fall to 1/e of the initial value, was 8.4 ns. (Fig. S10). After 1 ms, which is the time interval between the laser pulses (repetition rate = 1 kHz), the lattice temperature completely returns to initial temperature (ΔT_l< 10^{-5} K).

Accordingly, the heat accumulation by the laser pulse train is negligible. We speculate that the laser irradiation on nanotube surfaces created defects and metastable lattice structures inducing a driving force for coalescing neighbouring SWNTs without thermal side effects such as burn-out, aggregation, and substrate damage.

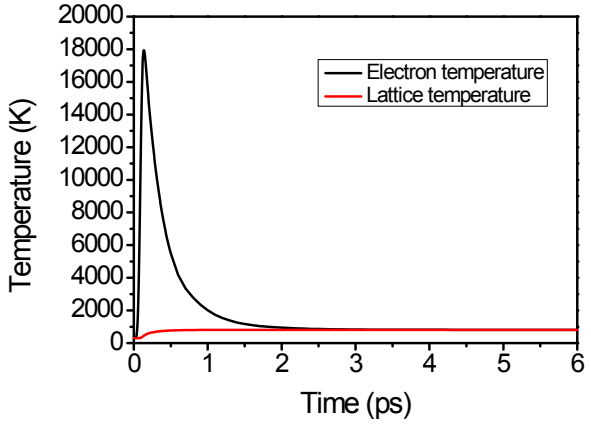

Figure S9 | Temporal evolution of electron and lattice temperatures.

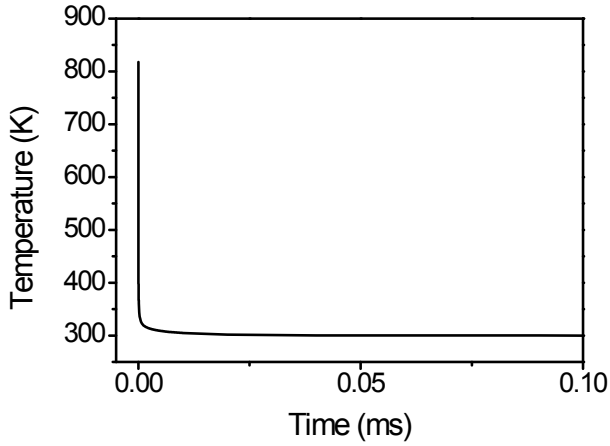

Figure S10 | Temporal evolution of lattice temperature after the equilibrium.

2.5 Effect of laser pulse width

Another laser system (laser pulse width = 250 fs, wavelength = 800 nm, repetition rate = 100 kHz) was employed to investigate the effect of laser pulse width. The relative CIM intensity was I_{CIM}/I_G = 0.26 at ~130 mJ/cm^2. The intensity ratio is lower than that obtained by 50 fs laser pulses (1.6) and similar to that obtained by thermal treatment.[11] Table S1 shows the CIM intensity ratio at different pulse widths.

Table S1 CIM intensity ratios obtained at different laser pulse widths

Laser pulse width	
50 fs	1.6
250 fs	0.26
25 ns[10]	0.09
Thermal[11]	0.26

References

[1] http://www.brewerscience.com/

[2] L. Jaber-Ansari, M. G. Hahm, S. Somu, Y. E. Sanz, A. Busnaina, and Y. J. Jung, *J. Am. Chem. Soc.* **2008**, *131*, 804.

[3] H. Y. Jung, P. T. Araujo, Y. L. Kim, S. M. Jung, X. T. Jia, S. Hong, C. W. Ahn, J. Kong, M. S. Dresselhaus, S. Kar, Y. J. Jung, *Nat. Commun.*, **2014**, 5.

[4] Y. Jiang, P. Wang, L. Lin *Nanotechnology* **2011**, *22*, 365704.

[5] D. Stauffer and A. Aharony, Introduction to Percolation Theory, 2nd ed. (Taylor & Francis, London, 1985)

[6] I. Chatzakis, *Appl. Phys. Lett.* **2013**, *103*, 043110.

[7] L. X. Benedict, *Solid State Commun.* **1996**, *100*, 177.

[8] A. H. Romero, M. E. Garcia, F. Valencia, H. Terrones, M. Terrones, and H. O. Jeschke, *Nano Lett.* **2005**, *5*, 1361.

[9] H. O. Jeschke, A. H. Romero, M. E. Garcia, and A. Rubio, *Phys. Rev. B* **2007**, *75.*

[10] A. P. Pino, E. Gyorgy, L. Cabana, B. Ballesteros, G. Tobias, *Carbon*, **2012**, 50, 4450.

[11] M. Endo, Y. A. Kim, T. Hayashi, H. Muramatsu, M. Terrones, R. Saito, F. Villalpando-Paez, S. G. Chou, M. S. Dresselhaus, *Small*, **2006**, 2, 1031-1036.